



# Quinazoline clubbed 1,3,5-triazine derivatives as VEGFR2 kinase inhibitors: design, synthesis, docking, in vitro cytotoxicity and in ovo antiangiogenic activity

Prateek Pathak<sup>1</sup> · Parjanya Kumar Shukla<sup>1</sup> · Vikas Kumar<sup>2</sup> · Ankit Kumar<sup>3</sup> · Amita Verma<sup>1</sup> 

Received: 21 December 2017 / Accepted: 23 March 2018  
© Springer International Publishing AG, part of Springer Nature 2018

## Abstract

A series of quinazoline clubbed 1,3,5-triazine derivatives (QCT) were synthesized and evaluated for their in vitro anticancer activity against HeLa (human cervical cancer), MCF-7 (human breast cancer cell), HL-60 (human promyelocytic leukemia cell), HepG2 (human Hepatocellular carcinoma cell), and one normal cell line HFF (human foreskin fibroblasts). In vitro assay result encouraged to further move towards in ovo anticancer evaluation using chick embryo. The series of QCT derivatives showed higher anticancer and antiangiogenic activity against HeLa and MCF-7 cell lines. In the series, synthetic molecule **8d**, **8l**, and **8m** displayed significant activity. Further, these results substantiated by docking study on VEGFR2. SAR study concluded that the potency of drugs depends on the nature of aliphatic substitution and the heterocyclic ring system.

**Keywords** MTT assay · Angiogenesis inhibition assay · 1,3,5-Triazine · Quinazoline derivative · VEGFR2 docking

## Introduction

In 2012, International Cancer Research Agency reported 14.1 million new cancer cases and 8.2 million deaths due to cancer (Jemal et al. 2011; Siegel et al. 2016). The agency propounds that global cancer burden will increase up to 21.7 million cases and 13 million deaths by the year 2030 (Singh et al. 2018). World Health Organization (WHO) official study emphasized that the toll of cancer (Kumar et al. 2017a) and other chronic diseases is higher in low- and middle economic countries (Verma et al. 2016, 2017b; Kumar et al. 2017b; Srivastava et al. 2017; Verma et al. 2017a). This

study showed the connection between economic status with chronic and non-curable disease (World Health Organization and WHO 2012; World Health Organization and Cancer Research UK 2014).

Angiogenesis is a fundamental and complex process of endothelial cells, pericytes and responsible to execute normal physiological responses (Carmeliet and Jain 2000). In normal conditions, controlled angiogenesis occurs during wound healing, embryonic development and in the female reproductive cycle. Whereas abnormal angiogenesis found in rheumatoid arthritis, psoriasis, diabetic retinopathy and tumorigenesis (Folkman 1995; Weis and Cheresh 2011). VEGFR<sub>2</sub> (KDR in human/Flk1 in mice) (Bergers and Benjamin 2003) is single pass transmembrane type 1 receptor protein, belongs to type III tyrosine kinase and VEGFR family. VEGFR<sub>2</sub> is responsible for development/proliferation, migration and survival of endothelial cells (Prager and Poettler 2011; Weis and Cheresh 2011). It is 230 kDa protein, expressed on the surface of endothelial cells and composed by N-terminal extracellular domain (seven immunoglobulin-like folds) (Tonini et al. 2003; Carmeliet 2005). Human VEGFR<sub>2</sub> gene located on Chromosome 4 (q11–q12) position (Folkman 2006; Prager and Poettler 2011). Judah Folkman and his colleagues established that angiogenesis has a vital role in tumorigenesis. Different studies also explain that in cancerous tumor formation, rapid sprouting of new fine

✉ Amita Verma  
amitaverma.dr@gmail.com; amita.verma@shiats.edu.in

<sup>1</sup> Bioorganic and Medicinal Chemistry Research Laboratory, Department of Pharmaceutical Sciences, Faculty of Health Sciences, Sam Higginbottom University of Agriculture, Technology and Sciences, Allahabad, Uttar Pradesh 211007, India

<sup>2</sup> Natural Product Drug Discovery Laboratory, Department of Pharmaceutical Sciences, Faculty of Health Sciences, Sam Higginbottom University of Agriculture, Technology and Sciences, Allahabad, Uttar Pradesh 211007, India

<sup>3</sup> Pharmaceutical Sciences, S. V. Subharti University, Meerut, India

capillaries occurs throughout the surroundings and accelerate the growth of tumor beyond 2–3 mm size. In this process, vascular endothelial growth factor (VEGF) pathways play an important role in their growth and metastatic potential (Folkman 2006; Yang et al. 2013). Thus, its inhibition is a prime target for various agents (Bjerkvig et al. 2009). In cancer biology, clinical applications of novel angiogenic inhibitors are limited due to modest efficiency and resistance (Bergers and Benjamin 2003; Folkman 2006; Nishida et al. 2006).

Biological applications of quinazoline and its derivatives identified through large no. of scientific communication during the second half of the twentieth century. Whereas second heterocycle 1,3,5-triazine and its derivatives reported as a potent skeleton for various therapeutic targets. Mono-, di- or tri-amino substituted 1,3,5-triazine conjugate such as tretamine, furazil and dioxadet have been reported as anticancer agents (Inomata et al. 2004). These therapeutic applications give us the brief idea that both of the nuclei can be utilized nicely towards designing of the novel anticancer agent. Thus, we adopted these as a significant factor and attempted to design, synthesis, docking, in vitro anticancer and antiangiogenic evaluation on cancer-induced chick embryo via the modification of quinazoline nucleus with 1,3,5-triazine. In the present work, designing of derivatives done on the basis of molecular field mapping, alignment and further compared with the standard angiogenic inhibitor vandetanib. The designed quinazoline clubbed 1,3,5-triazine (QCT) derivatives synthesized through cost-effective methodology and docking calculation is done on VEGFR2 protein model. The biological evaluation performed using MTT assay followed by cancer-induced angiogenesis inhibition in chick chorioallantoic membrane model (CAM).

## Experimental

Commercially available analytical grade solvents and reagents were used for the experiment without further purification. Melting points were determined by Veego, MPI melting point apparatus and uncorrected. FTIR ( $2.0\text{ cm}^{-1}$ , flat, smooth, abex) were recorded on Perkin Elmer RX-I Spectrophotometer.  $^1\text{H-NMR}$  and  $^{13}\text{C-NMR}$  spectra were recorded in  $\text{DMSO-}d_6$  using Bruker Avance II 400 and Bruker Avance II 100 NMR spectrometer, respectively, using TMS as an internal standard. Mass spectra were obtained on VG-AUTOSPEC spectrometer equipped with electrospray ionization (ESI) sources. Elemental analysis was carried out on Vario EL-III CHNOS elemental analyzer.

## Chemistry

The whole synthesis presented in the supplementary file.

## In vitro anticancer assay (cytotoxic study)

The QCT derivatives were the screen for their anticancer activity on four different cancer cell line HeLa (human cervical cancer), MCF-7 (human breast cancer cell), HL-60 (human promyelocytic leukemia cell), HepG2 (human hepatocellular carcinoma cell), and one normal cell line HFF (human foreskin fibroblasts).

## Cell culture

HeLa, MCF-7, HL-60, HepG2, and HFF cell lines were maintained in monolayer cultures in supplemented Dulbecco's modified Eagle's medium (DMEM) with 10% heat-inactivated fetal bovine serum (FBS), 1% L-glutamine, and 50  $\mu\text{g/ml}$  of gentamycin sulfate, at 37 °C, in  $\text{CO}_2$  incubator in an atmosphere of humidified 5%  $\text{CO}_2$  and 95% air (Wang et al. 2011).

## IC<sub>50</sub> value determination

Cells were seeded into 96-well microtiter plates. Each well was filled with 200  $\mu\text{l}$  of cell suspension ( $10^5$  cells/well) and cultured in DMEM, 10% FBS, 1% L-glutamine, and 50  $\mu\text{g/ml}$  gentamycin sulfate. The cells were incubated for 12 and 72 h with different concentrations of reference drug vandetanib and synthesized QCT derivatives. Untreated control cells were also included for each sample, which was maintained in DMEM and 5% FBS. The final concentration of DMSO used to solubilize synthesized derivatives and 0.1%, similar amount added to the control cells. The final concentration of ethanol was used to dissolve standard and 0.01%; a similar amount was added to the control cells. Cytotoxicity calculation of all derivatives and standard were determined using MTT (3-[4,5-dimethylthiazol-2-yl]-2,5-diphenyltetrazolium bromide) (Sigma) assay. The assay for selected concentration of sample (10–100  $\mu\text{g/ml}$  for initial trial; 10–30  $\mu\text{g/ml}$  in the second trial; 1–30  $\mu\text{g/ml}$  in the third trial) was performed in triplicate, and the culture plates were kept in 5% (v/v)  $\text{CO}_2$  humidified incubator at 37 °C for 24 and 72 h. Following that, 20  $\mu\text{l}$  of 0.5% w/v MTT, dissolved in phosphate-buffered (PBS) saline, was added to each well and further incubated for 4 h with 100  $\mu\text{l}$  of DMSO was added to each well and mixed vigorously to dissolve the formazan crystals. Absorbance values were determined using MRX II ELISA reader at 540 nm. All calculations were carried out in triplicates (Ahmadian et al. 2009; Patel and Patel 2011).

## In ovo antiangiogenic activity on cancer-induced CAM (Grodzik et al. 2011)

### Preparation of egg for xenograft

Fertilized eggs (204 nos.) from a local commercial hatchery guaranteeing 95% fertilization of the eggs were

purchased. Dirt, feathers and excrement were carefully removed from the eggshells mechanically by dry wiping with paper towels and 70% denatured ethanol (Sys et al. 2013). Eggs were incubated in a rotating incubator for 10 days at 100 °F and 60% humidity with rotation four times each hour. On a developmental day (10 days), the eggs were placed on their side in an egg rack. The chorioallantoic vein marked which is located at the top of the eggshell and junction of several large blood vessels. At this branch point, the blood vessel dropped down, away from the CAM and attached to the embryo 1 cm square box drawn with on the eggshell approximately 1 cm away from the branch point in the vein. A rotating cutting tool used to drill and make the window of pre-lined sample shell. A 25-gauge syringe needle with a fine bur on the end is used to make a small hole in the eggshell membrane being careful not to tear the underlying CAM. The CAM is subsequently detached from the eggshell membrane in the area of the square using gentle suction created with an automatic pipette aid fitted with a piece of ¼" tygon tubing placed against the hole in the air sac. Upon applying suction, an air pocket underneath the hole in the square signifies that the CAM has been successfully dropped away from the eggshell. After the CAM is dropped, the hole in the air sac and the hole located in the square near the chorioallantoic vein are sealed with a piece of laboratory tape. Subsequently (on day 8), the seal was removed and the discs (4 mm<sup>2</sup>) were placed on the chorioallantoic membrane of each egg. The seal has placed again and the eggs were then incubated for 24 h at 100 °F and 60% humidity in anticipation of grafting the tumor cells.

### Grafting of cancer cell line

Tumour cell detached from their culture dishes using EDTA and washed with 10 volumes of phosphate-buffered saline (PBS) to remove any residual media and all cell lines i.e., HeLa, MCF-7, HL-60, and HepG2 cancer cells (50 µL, 40,000 cells) were loaded individually on top of uncoated 12 µm ring inserts. The cells were allowed to migrate and invade to the lower chamber for 6 h. After 6 h of treatment, migration of cancer cells enhances the number of newly formed blood vessel branch points compared to phosphate-buffered saline (PBS)-treated control group. Each test compound was also analyzed for their ability to inhibit the growth of the tumor.

### Dosing

The measurement of the activity was done by counting only the blood vessels in the area under the disc. Each test

compound was prepared in stock solution and diluted with PBS in a concentration of 1.0 µM. 10 µL of this solution was added directly to the disc on top of CAM. The immunity of the chick embryo was found compromised and the life of CAM faced a challenge against higher dose (µg/ml) of tested and reference agent. Thus, we selected nmol concentration of the test as well as standard, i.e., 10 µl/CAM of drug concentration (1.0 µM), 0.01 nmol/CAM (Kue et al. 2015).

### Calculation of activity

The angiogenesis level was evaluated after that period by means of a stereomicroscope, by observing the vascular zone surrounding the disc. Antiangiogenic scores were calculated using given formula. Semi-quantitative score pattern such as 0=no or weak effect (more than 150 nos. of new vascularisation), 1=medium effect (in between 50 and 150 nos. of new vascularisation), and two or more considered as a strong effect (0–50 nos. of new vascularisation or capillary-free zone is at least twice as large as the pellet). The eggs in which the pellets caused inflammation and embryo-toxicity were excluded. Each experiment was performed in triplicate (Kıyan et al. 2013; Krenn and Paper 2009).

Average score =

$$\frac{\text{No. of egg (score 2)} \times 2 + \text{no. of eggs (score 1)} \times 1}{\text{Total no. of eggs (score 0, 1, 2)}}$$

### Molecular field mapping and alignment

Proteins respond to the potential field around a molecule rather than to the 3D arrangement of its individual atoms. The appearance of any molecule on any protein defines via a set of parameter properties near the molecular surface, not only the collection of atoms and bond. Any efficient descriptor consist steric and electrostatic phenomena of the molecules to understand biological activity through the interaction. Two molecules with different structures but similar biological activities present similar potential fields to their common binding site. As a result, they are expected to have similar sets of field points. This means that field patterns can be used to align molecules, to score active molecules (Cross and Cruciani 2010; Ou-Yang et al. 2012). Molecular field mapping and alignment of derivatives **8b**, **8d**, **8j**, **8m** on each other displayed in Fig. 1.

### Field point and its comparison

The fields described through scalar fields, which derived via calculation of interaction energy of a probe molecule with the target. Biological properties of a molecule in terms of a tractable number of field points used to compare structural

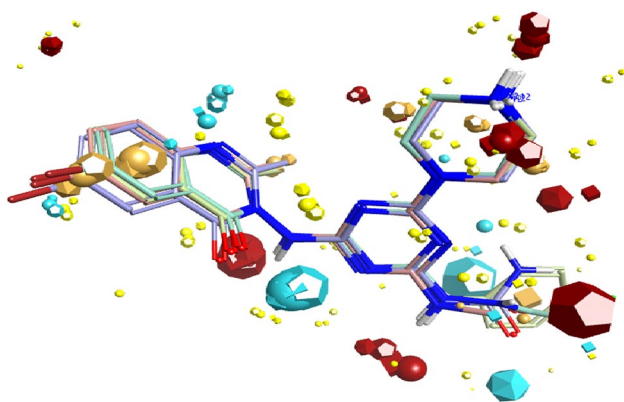


**Fig. 1** ADJM field template alignment of derivatives **8b**, **8d**, **8j**, **8m** on each other. Four different molecular fields represent binding properties of ligands with proteins, i.e., positive electrostatic interaction (red color), negative electrostatic interaction (blue color), Van der Waals attractive interaction steric (yellow color), and hydrophobic interaction (orange color) shown in figure. Field similarity, conformational analysis, alignment, 2D similarity, SlogP and TPSA value presented in Table 1 (color figure online)

diversity via chemical structure. We performed field analysis of the designed derivative and compared with known antiangiogenic compound vandetanib using FORZE V10 software. The field point alignment of quinazoline-clubbed 1, 3, 5- triazine derivatives (QCT) (**8b**, **8d**, **8j** and **8m**) on vandetanib is shown in Fig. 2. The field point generation is a sophisticated Pharmacophore and used to define a template for binding. Molecules overlaid calculation done using their fields, structural resemblance and field similarity between two molecules. This structural and field similarity quantified and transformed in a similarity value. This propounds that compounds having a parallel arrangement of field point, bind to the protein or receptor in similar pattern and affinity (Lengauer et al. 2004; Rollinger et al. 2008). The field similarity result calculations were mentioned in Table 1.

### Computational methodology

All the computational studies were carried out on a four CPUs (Intel Core2 Quad CPU Q9550 @ 2.83 GHz) ACPI x64 workstation with windows 8.1 operating system. We selected our targeted VEGFR2 kinase protein X-ray structure along with its ligand from Protein Data Bank (PDB id 3EWH). The protein sequence analyzed and handled with pymole 1.1 software. Water, bonded ligand and other heteroatom were removed (Pettersen et al. 2004). The structure of compounds **8b**, **8d**, **8j**, **8m** and vandetanib were prepared using MarvinSketch 5.5.0.1 software. The lowest energy conformations were determined at pH 7.0 with Open Babel 2.2.3 software using the MMFF94 s force field. Computational simulation studies have been performed with Auto dock 4.2. Essential hydrogen atoms, Kollman united atom

type charges, and solvation parameters were added with the aid of Auto dock tools. Affinity (grid) maps of  $20 \times 20 \times 20$  Å grid points and 0.375 Å spacing were generated using the Autogrid program. Auto dock parameter set- and distance-dependent dielectric functions were used in the calculation of the Vander Waal and the electrostatic terms, respectively. Computational simulations were performed using the Lamarckian genetic algorithm (LGA) and the Solis and Wets local search method. Initial position, orientation, and torsions of the ligand molecules were set randomly. Each docking experiment was derived from ten different runs that were set to terminate after a maximum of 250,000 energy evaluations. The population size was set to 150. During the search, a translational step of 0.2 Å, and quaternion and torsion steps of 5 were applied.

### Statistical analysis

All the data were expressed as the mean SEM and analysis of variance (one way ANOVA) was used for the statistical analysis using Graph Pad Prism version 5.0. The values were considered to be significant when the  $p$  value was  $\#p > 0.05$ .

## Result and discussion

### Chemistry

In this research, we synthesized quinazoline and substituted 1,3,5-triazine structures and clubbed both of them. Furthermore, we evaluate the anticancer potency of the derivatives. The designed substitution pattern of the series i.e., **8(a–o)** showed in Fig. 3. The designed product is synthesized by the multistep traditional organic chemistry protocol. Initially, mono-substituted anthranilic acid (**2**) was synthesized through bromination in controlled temperature condition. The adduct (**2**) undergoes acetylation and formed 6-Bromo-2-methyl-4H-benzo[d][1,3]oxazine (**3**). 6-bromo-2-methyl-4H-quinazolin-3-ylamine (**4**) was synthesized in the third synthetic step through conjugation with hydrazine hydrate under reflux.

The reaction protocol fourth step involved the formation of 4,6-dichloro-2-piperazin-1-yl-[1,3,5]triazine (**6**). This reaction was carried out in the presence of piperazine at the freezing condition. Furthermore, selected amine substituted on 1,3,5-triazine ring resulting 2,chloro-4,substitutedamino-6-piperazin-1-yl-[1,3,5]triazine (**7**) formed. The final synthetic scheme consist protocol consists nucleophilic substitution reaction resulting derivatives **8(a–o)** were formed. The structure of derivatives was established through spectroscopic (IR, Mass,  $^1\text{H-NMR}$  and  $^{13}\text{C-NMR}$ ) and elemental analysis.

A strong IR peak was recorded between the ranges  $3210\text{--}3240\text{ cm}^{-1}$  which confirmed the presence of  $\text{--NH}$

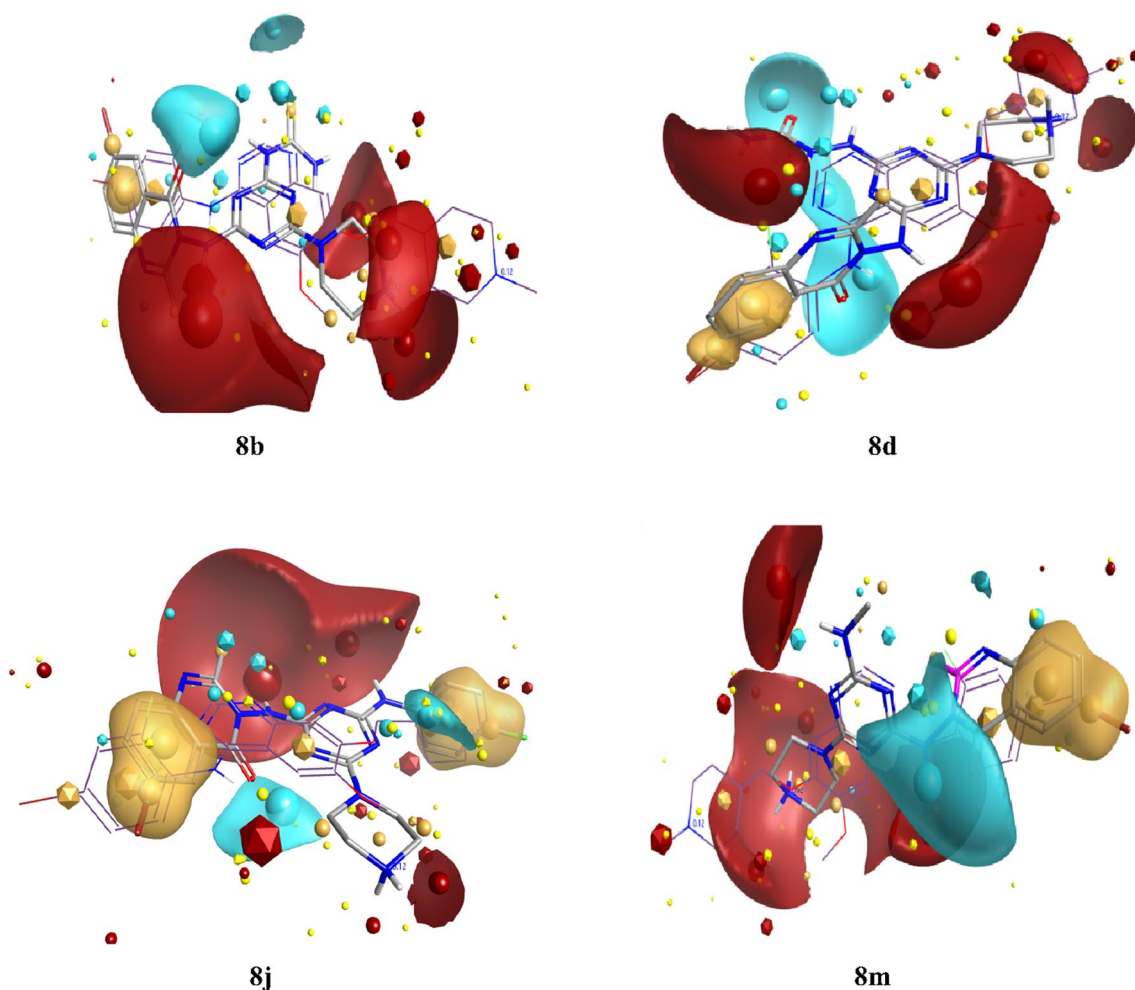


**Fig. 2** Field point alignment of quinazoline clubbed 1,3,5-triazine derivatives (QCT) (**8b**, **8d**, **8j** and **8m**) on vandetanib. The size of the point indicates the potential strength of the interaction. Round-shaped field points are test compounds: **8b**, **8d**, **8j** and **8m**. Diamond-shaped field points are reference compound (vandetanib). Sky blue color:

negative ionic fields; magenta color: positive ionic fields; light yellow color: vander waal interactions; dark yellow color: hydrophobic fields. Field similarity score, **8b**: 0.57; **8d**: 0.609; **8j**: 0.546, **8m**: 0.592 (color figure online)

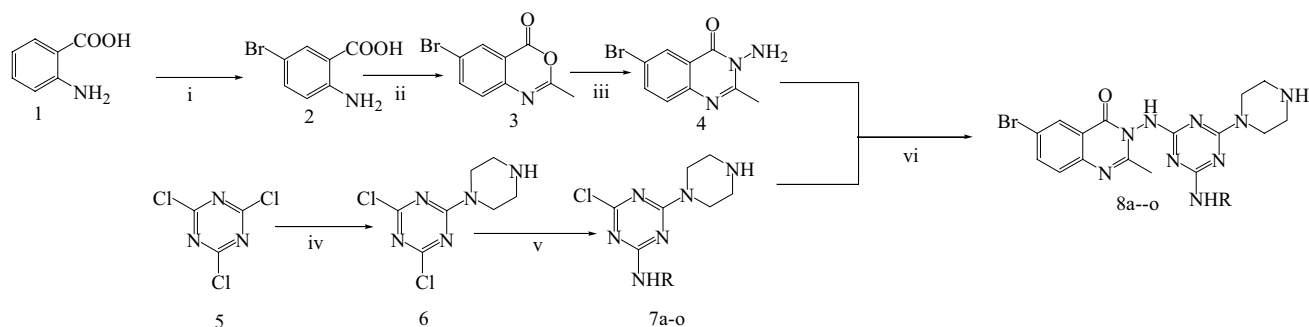
stretch. The aromatic  $-\text{CH}$  group of QCT derivative were observed  $2925\text{--}3050\text{ cm}^{-1}$ .  $\text{C}=\text{O}$  group peak in quinazoline ring was identified between the  $1610\text{--}1795\text{ cm}^{-1}$  range. Presence of Br group confirmed via strong band appears from  $705\text{--}755\text{ cm}^{-1}$ .  $^1\text{H-NMR}$  of the entire derivative showed a singlet in the range at  $\delta$  2.22–2.35 attributed to the presence of a  $\text{CH}_3$  proton on quinazoline.  $^1\text{H-NMR}$  also showed another multiplet at  $\delta$  3.05–3.85 ppm represented piperazine and four quinazoline protons between 4.46 and 8.28  $\delta$  ppm. The  $^{13}\text{C-NMR}$  showed carbon signals between 20.22 and 187.11 ppm which confirm quinazoline, triazine ring, and an aliphatic chain. Eventually, all the structure of synthesized derivatives was found in accordance with mass and elemental analysis.

### Anticancer activity

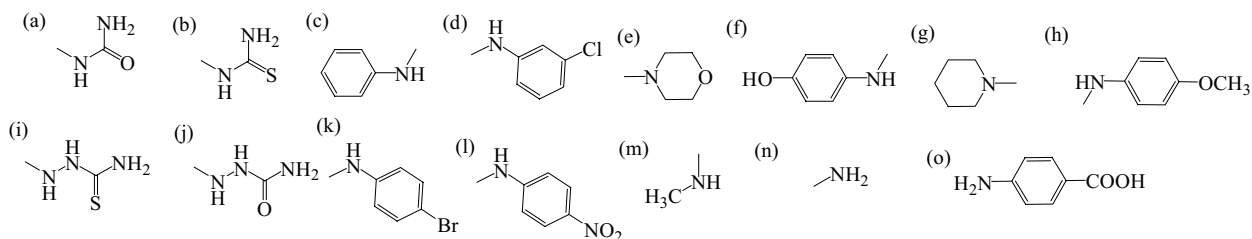
In vitro cytotoxicity of newly synthesized derivatives (**8a–o**) was measured by MTT [3-(4,5-dimethyl thiazolyl-2)-2,5-diphenyltetrazolium bromide] assay against cell lines, namely HeLa (human cervical cancer), MCF-7 (human breast cancer cell), HL-60 (human promyelocytic leukemia cell) and HepG2 (human hepatocellular carcinoma cell), and HFF (human foreskin fibroblasts). All the cell lines were procured from NCCS, Pune (India). Vandetanib, a most significant anticancer agent was used as a reference drug in the study. Survival curve for the tested cell lines HeLa, MCF-7, HL-60, and HepG2 was obtained by plotting graph between

**Table 1** Field similarity and alignment data of the designed quinazoline derivatives

SN	Titled compound	Similarity	No. of confs	Alignments	2D similarity	SlogP	TPSA
1	<b>8a</b>	0.570	39	10	0.217	1.1	158.3
2	<b>8b</b>	0.571	50	10	0.217	1.3	141.3
3	<b>8c</b>	0.565	35	10	0.247	3.4	115.3
4	<b>8d</b>	0.609	46	10	0.24	4.1	115.3
5	<b>8e</b>	0.560	16	10	0.22	1.5	115.7
6	<b>8f</b>	0.551	50	10	0.24	3.1	135.5
7	<b>8g</b>	0.563	20	10	0.223	2.6	106.5
8	<b>8h</b>	0.564	50	10	0.262	3.4	124.5
9	<b>8i</b>	0.539	50	10	0.205	0.8	153.3
10	<b>8j</b>	0.546	50	10	0.205	0.6	170.4
11	<b>8k</b>	0.556	39	10	0.247	4.2	115.3
12	<b>8l</b>	0.592	39	10	0.228	3.2	161.1
13	<b>8m</b>	0.592	21	10	0.245	1.7	115.3
14	<b>8n</b>	0.59	16	10	0.232	1.2	129.2
15	<b>8o</b>	0.55	48	10	0.23	-0.7	155.4
16	Vandetanib	–	–	–	1.00	5.3	60.7

**Reaction scheme:**

where R =

**Reaction conditions and reagents:**

(i) Glacial acetic acid, bromine in acetic acid solution, benzene, HCl (ii) Acetic anhydride, reflux for 4 hrs (iii) Hydrazine hydrate, pyridine, reflux for 3 hrs. (iv) Piperazine, Acetone, NaHCO<sub>3</sub> solution (10%), stir for 3-4 hrs below 5<sup>0</sup>C (v) Amines, acetone, NaHCO<sub>3</sub> solution (10%), stir for 4 hrs at room temp (vi) 1,4-dioxane, K<sub>2</sub>CO<sub>3</sub>, reflux for 8-10 hrs

**Fig. 3** Reaction scheme for designed synthesis of the quinazoline derivatives

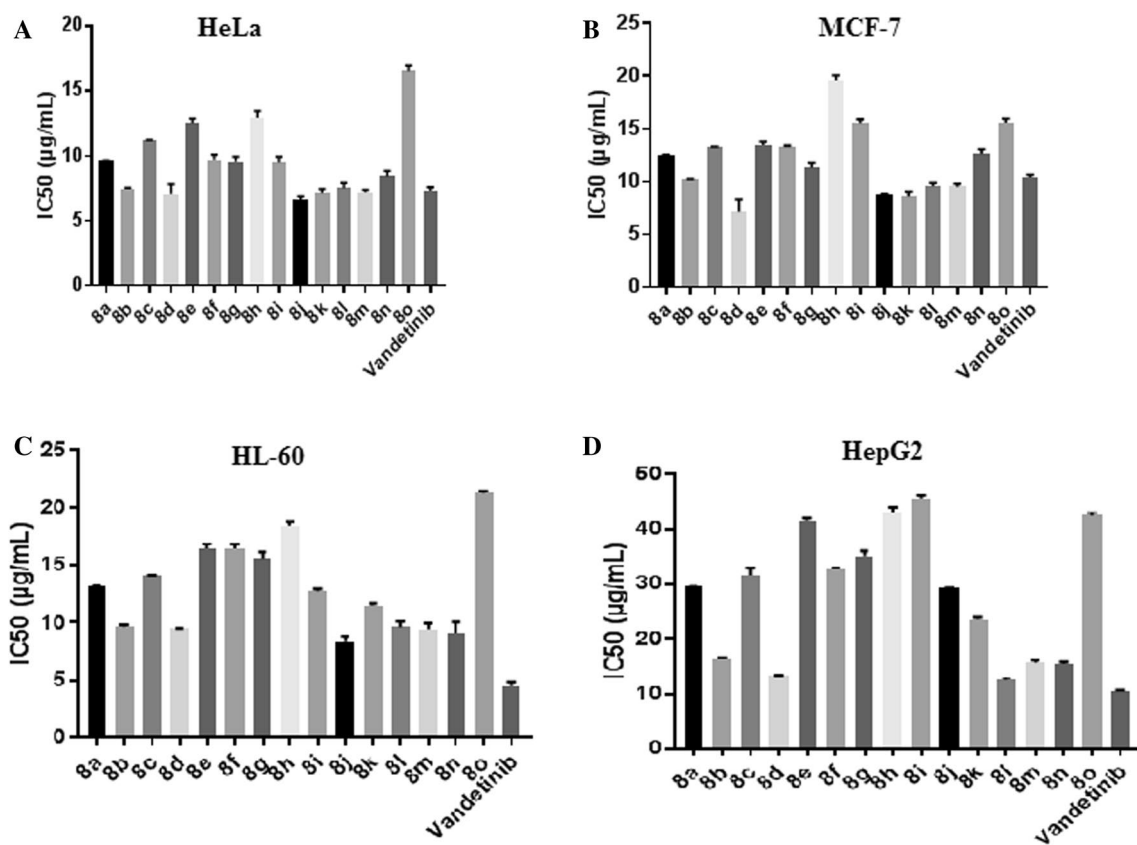


**Fig. 4** Image a, b, c, and d refers the in vitro anticancer activity against HeLa, MCF-7, HL-60, and HepG2 cell lines. The graph displayed between IC<sub>50</sub> vs. derivatives (Y-axis shows 50% inhibitory

concentration, while on X-axis different synthesized derivatives 8(a-o) and reference drug vandetanib are shown)

**Table 2** In vitro anticancer activity (IC<sub>50</sub> = mean ± SD) of the synthesized quinazoline derivatives

Titled compound	HeLa (IC <sub>50</sub> µM)	MCF-7 (IC <sub>50</sub> µM)	HL-60 (IC <sub>50</sub> µM)	HepG2 (IC <sub>50</sub> µM)	HFF (IC <sub>50</sub> µM)
8a	09.61 ± 0.011****	12.45 ± 0.09****	13.13 ± 0.06****	29.45 ± 0.18****	Non-toxic
8b	07.48 ± 0.06#	10.22 ± 0.02#	09.65 ± 0.13****	16.52 ± 0.02****	Non-toxic
8c	11.22 ± 0.02****	13.29 ± 0.02****	14.11 ± 0.01****	31.61 ± 1.25****	Non-toxic
8d	07.08 ± 0.76#	07.16 ± 1.17****	09.48 ± 0.02****	13.25 ± 0.08****	Non-toxic
8e	12.5 ± 0.39****	13.4 ± 0.30****	16.47 ± 0.36****	41.59 ± 0.39****	79.16 ± 0.01
8f	09.7 ± 0.39****	13.25 ± 0.14****	16.47 ± 0.34****	32.63 ± 0.32****	Non-toxic
8g	09.55 ± 0.37****	11.32 ± 0.45#	15.51 ± 0.67****	35.07 ± 0.88****	88.64 ± 0.42
8h	12.94 ± 0.50****	19.57 ± 0.50****	18.45 ± 0.30****	43.01 ± 0.86****	Non-toxic
8i	09.50 ± 0.41****	15.51 ± 0.39****	12.78 ± 0.17****	45.51 ± 0.50****	72.68 ± 0.28
8j	06.65 ± 0.23#	08.69 ± 0.13***	08.40 ± 0.37****	29.35 ± 0.20****	Non-toxic
8k	07.13 ± 0.33#	08.61 ± 0.43***	11.56 ± 0.14****	23.54 ± 0.40****	Non-toxic
8l	07.52 ± 0.40#	09.54 ± 0.33#	09.60 ± 0.49****	12.47 ± 0.37**	Non-toxic
8m	07.21 ± 0.17#	09.52 ± 0.27#	09.45 ± 0.48****	15.61 ± 0.44****	Non-toxic
8n	08.42 ± 0.043*	12.62 ± 0.44****	09.08 ± 0.94****	15.43 ± 0.34****	Non-toxic
8o	16.53 ± 0.42****	15.54 ± 0.41****	21.27 ± 0.17****	42.42 ± 0.51****	Non-toxic
Vandetanib	07.31 ± 0.27	10.42 ± 0.22	04.48 ± 0.41	10.51 ± 0.14	Non-toxic

SD standard deviation, \* *p* < 0.05, \*\* *p* < 0.01, \*\*\* *p* < 0.001, \*\*\*\* *p* < 0.0001, # *p* > 0.05 in comparison with vandetanib (Dunnett's *t* test)

**Table 3** In ovo antiangiogenic activity score (score  $\pm$  SD) of synthesized derivatives on HeLa, MCF-7, HL-60 and HepG2

Titled compound	Conc (nM)	HeLa	MCF-7	HL-60	HepG2
<b>8a</b>	0.01	1.53 $\pm$ 0.07 <sup>****</sup>	1.13 $\pm$ 0.06 <sup>****</sup>	1.24 $\pm$ 0.02 <sup>****</sup>	0.99 $\pm$ 0.02 <sup>****</sup>
<b>8b</b>	0.01	1.58 $\pm$ 0.06 <sup>****</sup>	1.25 $\pm$ 0.08 <sup>****</sup>	0.99 $\pm$ 0.06 <sup>****</sup>	0.98 $\pm$ 0.02 <sup>****</sup>
<b>8c</b>	0.01	1.16 $\pm$ 0.06 <sup>****</sup>	1.12 $\pm$ 0.02 <sup>****</sup>	1.1 $\pm$ 0.02 <sup>****</sup>	0.99 $\pm$ 0.01 <sup>****</sup>
<b>8d</b>	0.01	1.94 $\pm$ 0.02 <sup>#</sup>	1.90 $\pm$ 0.01 <sup>#</sup>	1.32 $\pm$ 0.03 <sup>****</sup>	0.98 $\pm$ 0.02 <sup>****</sup>
<b>8e</b>	0.01	Toxic	0.22 $\pm$ 0.02 <sup>****</sup>	Toxic	0.49 $\pm$ 0.02 <sup>****</sup>
<b>8f</b>	0.01	1.02 $\pm$ 0.08 <sup>****</sup>	1.02 $\pm$ 0.08 <sup>****</sup>	1.08 $\pm$ 0.13 <sup>****</sup>	0.09 $\pm$ 0.08 <sup>****</sup>
<b>8g</b>	0.01	Toxic	1.74 $\pm$ 0.07 <sup>#</sup>	0.89 $\pm$ 0.18 <sup>****</sup>	Toxic
<b>8h</b>	0.01	0.60 $\pm$ 0.08 <sup>****</sup>	0.89 $\pm$ 0.01 <sup>****</sup>	0.97 $\pm$ 0.005 <sup>****</sup>	1.00 $\pm$ 0.02 <sup>****</sup>
<b>8i</b>	0.01	1.23 $\pm$ 0.10 <sup>****</sup>	1.03 $\pm$ 0.06 <sup>****</sup>	0.97 $\pm$ 0.04 <sup>****</sup>	0.86 $\pm$ 0.01 <sup>****</sup>
<b>8j</b>	0.01	1.91 $\pm$ 0.01 <sup>#</sup>	1.19 $\pm$ 0.06 <sup>****</sup>	0.89 $\pm$ 0.07 <sup>****</sup>	0.70 $\pm$ 0.05 <sup>****</sup>
<b>8k</b>	0.01	1.03 $\pm$ 0.07 <sup>****</sup>	1.08 $\pm$ 0.05 <sup>****</sup>	0.74 $\pm$ 0.04 <sup>****</sup>	0.94 $\pm$ 0.03 <sup>****</sup>
<b>8l</b>	0.01	1.84 $\pm$ 0.02 <sup>#</sup>	1.84 $\pm$ 0.04 <sup>#</sup>	1.25 $\pm$ 0.06 <sup>****</sup>	0.98 $\pm$ 0.02 <sup>****</sup>
<b>8m</b>	0.01	1.82 $\pm$ 0.07 <sup>#</sup>	1.85 $\pm$ 0.03 <sup>#</sup>	1.29 $\pm$ 0.03 <sup>****</sup>	0.63 $\pm$ 0.04 <sup>****</sup>
<b>8n</b>	0.01	1.11 $\pm$ 0.09 <sup>****</sup>	0.98 $\pm$ 0.03 <sup>****</sup>	1.07 $\pm$ 0.05 <sup>****</sup>	0.62 $\pm$ 0.02 <sup>****</sup>
<b>8o</b>	0.01	0.98 $\pm$ 0.02 <sup>****</sup>	1.34 $\pm$ 0.01 <sup>****</sup>	1.15 $\pm$ 0.04 <sup>****</sup>	0.64 $\pm$ 0.03 <sup>****</sup>
Control (PBS)	0.01	0.1 $\pm$ 0.1	0.1 $\pm$ 0.1	0.1 $\pm$ 0.1	0.1 $\pm$ 0.1
Vandantib	0.01	1.87 $\pm$ 0.03	1.87 $\pm$ 0.02	1.72 $\pm$ 0.07	1.33 $\pm$ 0.07

SD standard deviation, \*\*\* $p$  < 0.001, \*\*\*\* $p$  < 0.0001, # $p$  > 0.05 in comparison with vandetanib (Dunnett's  $t$  test)

survival fractions versus drug concentration. Anticancer activities of the derivatives are illustrated in Fig. 4. The potency was defined in terms of IC<sub>50</sub> value which showed the concentration of the drug for 50% inhibition of cell viability. The in vitro anticancer potency of the synthesized derivatives is displayed in Table 2.

Anticancer activity of the QCT derivatives was performed and compared with standard drug vandetanib. Our synthesized derivatives **8a–o** expressed IC<sub>50</sub> ranging from 06.65  $\pm$  0.23–45.51  $\pm$  0.50  $\mu$ M. The results of the present study displayed that the tested derivatives were found active against all investigated human cancer cell lines. Few derivatives were found significantly active against HeLa and MCF-7 cell lines. The results explained that the derivatives such as **8b**, **8g**, **8l**, and **8m** have shown remarkable inhibitory activities against HeLa cell line. However, derivatives viz. **8b**, **8d**, **8j**, **8k**, **8l**, and **8m** displayed remarkable activity against MCF-7 cell line as compared to the standard drug, vandetanib.

Results showed that urea substitution on 1,3,5-triazine ring renders the derivative marginal ( $p$  < 0.0001) active against HeLa (IC<sub>50</sub> 09.61  $\pm$  0.011), MCF-7 (IC<sub>50</sub> 12.45  $\pm$  0.09), HL-60 (IC<sub>50</sub> 29.45  $\pm$  0.18), and HepG2 (IC<sub>50</sub> 13.13  $\pm$  0.06) cell lines. Surprisingly, the introduction of thiourea on the skeleton of 1,3,5-triazine derivative **8b** showed significant ( $p$  > 0.05) activity against HeLa (IC<sub>50</sub> 07.48  $\pm$  0.06) and MCF-7 (IC<sub>50</sub> 10.22  $\pm$  0.02  $\mu$ M) cell line in comparison to reference drug. However, incorporation of 4-anilino with 1,3,5-triazine led to significant

decrease activity in **8c**. IC<sub>50</sub> values were observed as 11.22  $\pm$  0.02  $\mu$ M (HeLa cells), 13.29  $\pm$  0.02  $\mu$ M (MCF-7 cells), 14.11  $\pm$  0.01  $\mu$ M (HL-60 cells), and 31.61  $\pm$  1.25  $\mu$ M (HepG2). To our astonishment, the activity was significantly ( $p$  > 0.05) increased against HeLa 07.08  $\pm$  0.76  $\mu$ M, on the introduction of color-anilino at 1,3,5-triazine ring, derivative **8d**. Major declension in anticancer potency was reported for derivatives **8e** and **8f** against HeLa, MCF-7, HL-60, and HepG2 cancer cell lines. Piperidine substitution on 1,3,5-triazine skeleton derivative **8g** remarkably found active against MCF-7 [IC<sub>50</sub> 11.32  $\pm$  0.45  $\mu$ M ( $p$  > 0.05)]. The presence of methoxy and carbothioamide substituent at 1,3,5-triazine significantly decreases the activity against all cell lines, derivatives **8h**, **8i**. A sudden increase in activity was reported against HeLa by derivative **8j**, **8k**, **8l**, and **8m** possess hydrazinecarboxamide, Br-Ph, Nitro-Ph, and methylamino substitution on 1,3,5-triazine, whereas **8l** and **8m** were found significantly active against MCF-7 cell line. The IC<sub>50</sub> of derivatives **8j**, **8k**, **8l**, and **8m** were displayed as 6.65  $\pm$  0.23, 7.13  $\pm$  0.33, 7.52  $\pm$  0.40, 7.21  $\pm$  0.17  $\mu$ M ( $p$  > 0.05) against HeLa cell line, whereas **8l**, and **8m** showed remarkable effect with IC<sub>50</sub> value as 09.54  $\pm$  0.33, 09.52  $\pm$  0.27  $\mu$ M ( $p$  > 0.05) against MCF-7 cell line. Marginal anticancer activity was found in amino substituted 1,3,5-triazine derivatives **8n** against HeLa [IC<sub>50</sub> 08.42  $\pm$  0.043  $\mu$ M, ( $p$  < 0.05)].

The anticancer assay showed that derivative **8j** acts as the most active molecule against HeLa, while derivative **8d** has the maximum potency against MCF-7. The above results also

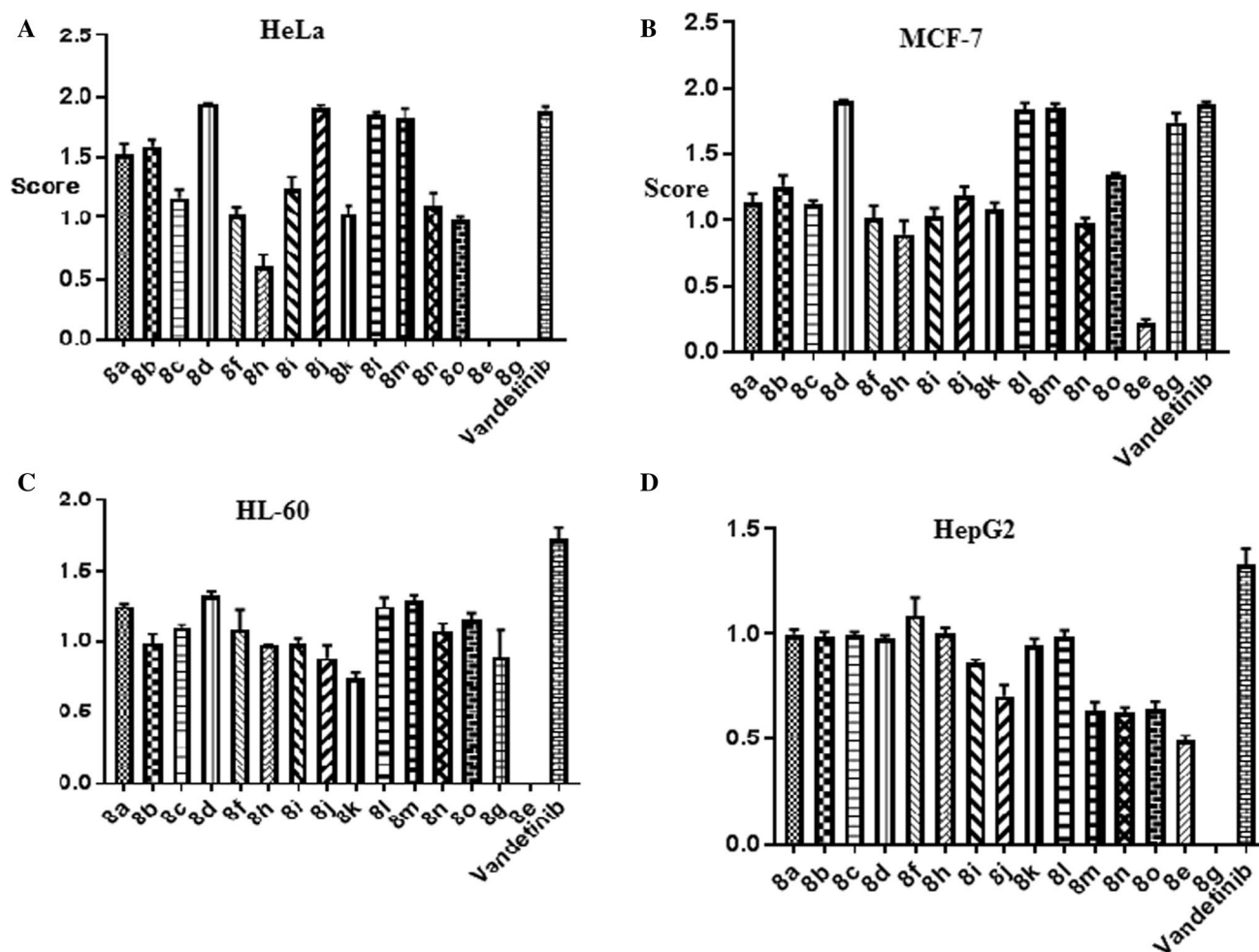


**Fig. 5** Image **a**, **b**, **c**, and **d** refers the graph of antiangiogenic activity in cancer-induced chick embryo. Y-axis shows inhibitory score, however, on X-axis different synthesized derivatives **8(a–o)** and reference drug vandetanib are shown

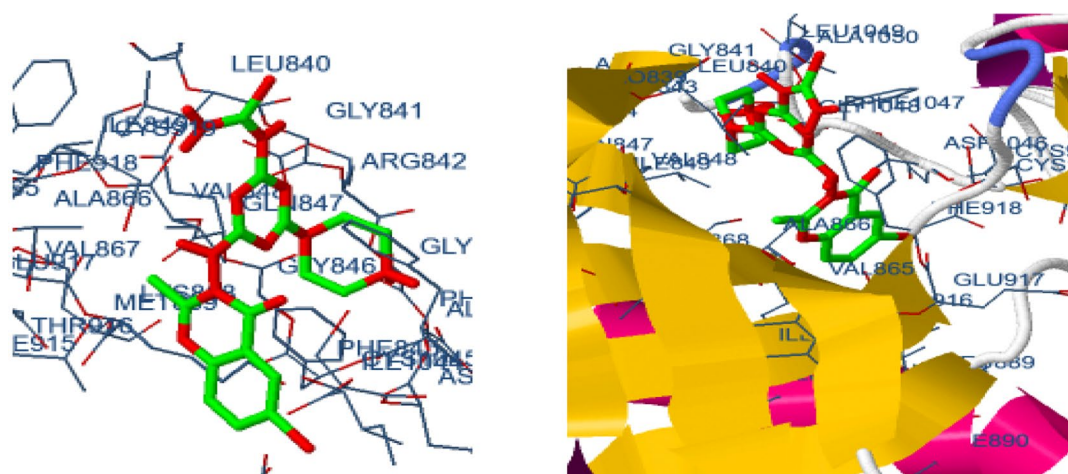
showed that the entire series of derivative has some anticancer potency. The SAR study revealed that both aromatic and aliphatic nucleophile makes the contribution to biological activity. The presence of hydroxy and methoxy group on phenyl ring system endangers the anticancer potential, while the introduction of halogen on phenyl ring improves the anticancer activity. To decide the selectivity of these derivatives among normal and cancerous cells, the designed derivatives were also tested against HFF, a normal human foreskin fibroblast cell. The outcomes showed that most of the molecules were found non-toxic to the normal cell (data not shown).

### In vivo antiangiogenic pharmacology

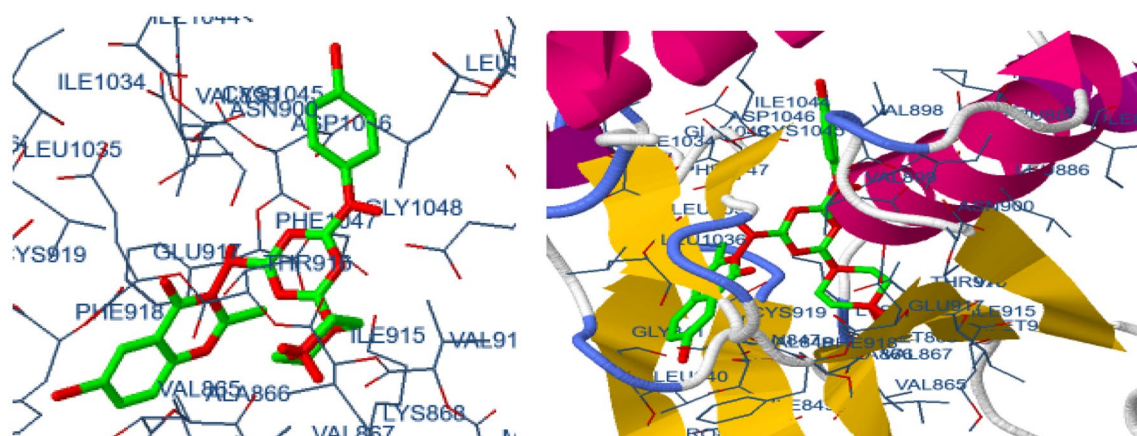
The synthesized QCT derivatives were evaluated in ovo for antiangiogenic activity (0.01 nM) and the results obtained were reported as score in comparison to vandetanib as a reference. The angiogenesis inhibition score was displayed

in Table 3, whereas the graphical bar presentation of activity displayed in Fig. 5. The QCT derivatives (**8a–o**) expressed mild to moderate angiogenesis inhibition score as  $0.22 \pm 0.02$ – $1.91 \pm 0.01$  against HeLa, MCF-7, HL-60, and HepG2 cell line-induced chick embryo. Entire synthesized derivatives were found active against all tested cell lines. The derivative **8a** and **8c** showed considerable activity against HeLa-induced egg, whereas marginal activity was found against MCF-7-, HL-60-, and HepG2 cell-induced chick embryo. QCT derivative **8c** was found marginally active. To our surprise, in **8d** inhibition score was significantly ( $p > 0.05$ ) increased against MCF-7- and HeLa-induced ova with a score of  $1.94 \pm 0.02$  and  $1.90 \pm 0.01$ , respectively. The derivatives **8e–i** found to possess marginal activity except for **8g**. The derivative **8g** showed significant ( $p > 0.05$ ) activity against MCF-7 cell-induced egg (Score of  $1.74 \pm 0.07$ ). The compound **8j** showed promising activity ( $1.91 \pm 0.01$ ) ( $p > 0.05$ ) against HeLa-induced egg cell, whereas marginal

8b:



8d:



8j

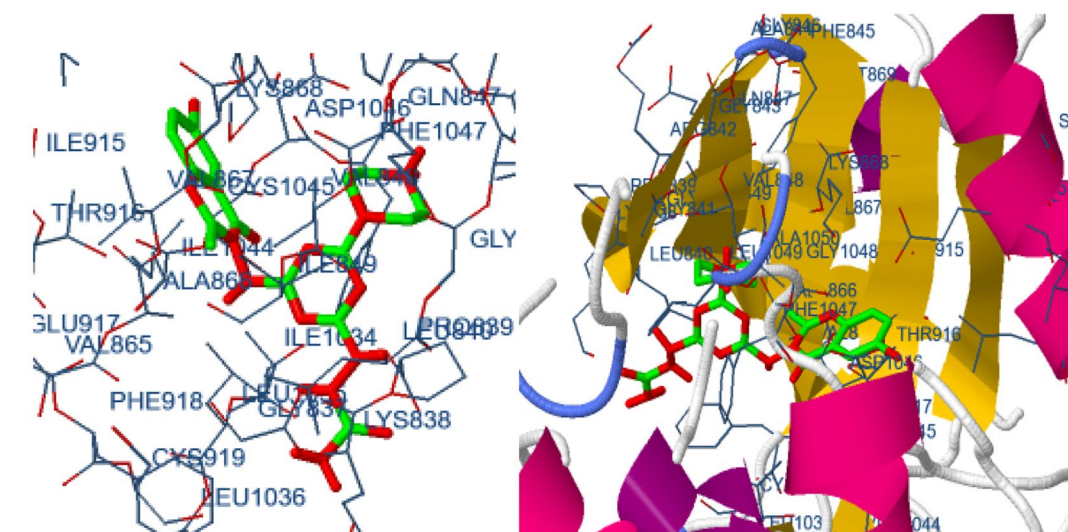


**Fig. 6** Docking of compounds (**8b**, **8d**, and **8j**) into the active site of VEGFR2 kinase domain (3EWH) showed the interaction side chain (in red) of amino acid (color figure online)

**Table 4** Docking study of synthesized derivation against 3EWH protein

Titled compound	H bond	Est. free binding energy (kcal/mol)	Inhibition const (K) ( $\mu\text{M}$ )	vdW + Hbond + des-olv energy (kcal/mol)	Electro-static energy (kcal/mol)	Int.mole energy (kcal/mol)	Freq.	Total interacting surface
<b>8b</b>	N9—LEU840 (2.96A) N8—PHE1047(2.58A) O1-CYS1045 (3.53A)	-7.77	2.02	-8.64	+0.10	-8.54	50%	952.693
<b>8d</b>	N9—ALA866 (2.54A) N9—VAL914 (2.57A) N9—THR916 (3.35A) N5—GLU885 (2.89A) N7—GLU885 (2.64A)	-9.57	97.05	-9.94	-0.14	-10.08	80%	1055.456
<b>8j</b>	N7—LEU840 (3.07A) N10—LEU840 (2.58A) N11—LEU840 (3.32A) N9-GLU917 (2.80A)	-9.93	1.55	-8.50	-0.16	-8.34	60%	967.249
<b>8m</b>	N7(20)—LEU840 (3.30A) N1(7)—THR916 (3.25A) N9(24)—GLU917 (2.56A) H14(42)—ALA866 (2.57A) H14(42)—THR916 (3.49A) H13(41)—CYS919 (3.76A) H8(36)—PHE1047 (3.46A)	-7.97	1.43	-8.17	-0.17	-8.27	50%	835.14
Ref.	N2—THR916 (2.76A) N3—THR916 (3.42A)	-7.70	2.29	-9.03	+0.21	-882	10%	94.10

score against MCF-7, HL-60, and HepG2 cancer cells. The derivatives **8l** and **8m** were found significantly ( $p > 0.05$ ) active against HeLa- and MCF-7-induced chick ova. **8l** exhibited activity score  $1.84 \pm 0.02$ ,  $1.84 \pm 0.04$ , whereas **8k** showed  $1.82 \pm 0.07$ ,  $1.85 \pm 0.03$  ( $p > 0.05$ ) against HeLa- and MCF-7-induced chick embryo, respectively. The result showed that synthesized derivatives **8d**, **8j**, **8l**, and **8m** demonstrated significant activity against HeLa, while **8d**, **8g**, **8l**, and **8m** against MCF-7-induced egg, respectively. The findings of the angiogenesis inhibition assay were found to be comparable to that of in vitro outcomes.

### Molecular docking study

The designed derivatives docked to the VEGFR2 domain. Docking interaction of compounds (**8b**, **8d**, and **8j**) into the active site of VEGFR2 kinase domain displayed in

Fig. 6. The result obtained from docking can be utilized to establish and validate our results. A conclusion of the docking results evaluated via the comparison of binding energy and inhibition constant between the designed derivatives and vandetanib. Genetic algorithm and in silico approach-based study were performed in the present paper. The result outcomes of derivatives **8b**, **8d**, **8j**, and **8m** are shown in Table 4. The result showed that QCT derivatives (**8b**), H-bond interacted with LEU840, PHE1047, and CYS1045, while **8d** exhibited H-bond interaction with ALA866, VAL914, THR916, and GLU885. Derivative **8j** explored H-bond interactions with LEU840, N9-GLU917. Furthermore, quinazoline derivative **8m** has the intensity to form H interaction with LEU840, THR916, GLU917, ALA866, THR916, CYS919, and PHE1047. Reference drug vandetanib showed hydrogen bond interactions with THR916. The amino acid residue THR916 showed

common interaction in **8d**, **8m**, and vandetanib. On comparing the results of docked ligands, we observed that **8b**, **8d**, **8j**, and **8m** have lower estimated binding energy than vandetanib. Whereas derivatives **8b**, **8j**, and **8m** have a lower inhibition constant than vandetanib as higher negative binding energy (kcal/mol) corresponds to the binding affinity. The top ligands **8b**, **8j**, and **8m** showed free binding energy 7.77,  $-9.93$  and  $-7.97$  kcal/mol, respectively. The observation based on lower free-binding energy, improved electrostatic interaction, and lower inhibition constant against VGFR2, we came to know that **8b**, **8j** and **8m** are the effective VGFR2 inhibitor. The interaction statistics also approved that **8b**, **8j**, and **8m** have maximum tendency to form hydrogen bonds in the hydrophobic pocket within the receptor as compared to other ligands.

## Conclusion

In the present communication, we had drawn the synthesis of novel heterocyclic QCT derivatives. The synthesized derivatives evaluated via in vitro anticancer activity and further in ovo cancer-induced angiogenesis inhibition. The in vitro and in ovo activity results revealed that most of the synthesized derivatives were active against HeLa and MCF-7 cancer types. The survival results of the eggs also explained that most of the compounds are non-toxic in nature and can proceed for further. The results also show that compounds **8d**, **8l**, and **8m** were the most promising anticancer agents with minimum  $IC_{50}$  value. SAR analysis put detail outline about the role of functional group that electron-withdrawing group modified biological activity through increased plasma protein binding due to balanced SlogP value and better topological surface area. Molecular docking studies of synthesized derivatives revealed that they have a tendency to bind with a narrow hydrophobic pocket of the N-terminal chain in the ATP binding site of EGFR. This study is understandable for further designing of diverse QCT-based heterocyclic derivatives and can provide new templates for antitumor chemotherapy. We could probably lead towards more active molecules in the area of cancer chemotherapy.

**Acknowledgements** The authors are thankful to the Department of Pharmaceutical Sciences, FHS, SHUATS, Allahabad for providing essential facility and support to perform this study. The author also acknowledged to Dr. Sachin Sakat for statistical analysis.

## Compliance with ethical standards

**Conflict of interest** The authors have declared that there is no conflict of interest.

## References

- Ahmadian S, Barar J, Saei AA, Fakhree MA, Omid Y (2009) Cellular toxicity of nanogenomedicine in MCF-7 cell line: MTT assay. *J Vis Exp* 26:e1191. <https://doi.org/10.3791/1191>
- Bergers G, Benjamin LE (2003) Angiogenesis: tumorigenesis and the angiogenic switch. *Nat Rev Cancer* 3:401–410. <https://doi.org/10.1038/nrc1093>
- Bjerkvig R, Johansson M, Miletic H, Niclou SP (2009) Cancer stem cells and angiogenesis. *Semin Cancer Biol* 19:279–284
- Carmeliet P (2005) VEGF as a key mediator of angiogenesis in cancer. *Oncology* 69:4–10
- Carmeliet P, Jain RK (2000) Angiogenesis in cancer and other diseases. *Nature* 407:249–257. <https://doi.org/10.1038/35025220>
- Cross S, Cruciani G (2010) Molecular fields in drug discovery: getting old or reaching maturity? *Drug Discov Today* 15:23–32
- Folkman J (1995) Angiogenesis in cancer, vascular, rheumatoid and other disease. *Nat Med* 1:27–31. <https://doi.org/10.1038/nm0195-27>
- Folkman J (2006) Angiogenesis. *Annu Rev Med* 57:1–18. <https://doi.org/10.1146/annurev.med.57.121304.131306>
- Grodzick M, Sawosz E, Wierzbicki M et al (2011) Nanoparticles of carbon allotropes inhibit glioblastoma multiforme angiogenesis in ovo. *Int J Nanomed* 6:3041–3048. <https://doi.org/10.2147/IJN.S25528>
- Inomata H, Goushi K, Masuko T et al (2004) High-efficiency organic electrophosphorescent diodes using 1,3,5-triazine electron transport materials. *Chem Mater* 16:1285–1291. <https://doi.org/10.1021/cm034689t>
- Jemal A, Bray F, Center MM et al (2011) Global cancer statistics. *CA Cancer J Clin* 61:69–90. <https://doi.org/10.3322/caac.20107>
- Kıyan HT, Demirci B, Kemal Hüsni Can Başer KH et al (2014) The in vivo evaluation of anti-angiogenic effects of Hypericum essential oils using the chorioallantoic membrane assay. *Pharm Biol* 52(1):44–50. <https://doi.org/10.3109/13880209.2013.810647>
- Krenn L, Paper DH (2009) Inhibition of angiogenesis and inflammation by an extract of red clover (*Trifolium pratense* L.). *Phytomedicine* 16:1083–1088. <https://doi.org/10.1016/j.phymed.2009.05.0177>
- Kue CS, Tan KY, Lam ML et al (2015) Chick embryo chorioallantoic membrane (CAM): an alternative predictive model in acute toxicological studies for anti-cancer drugs. *Exp Anim* 64(2):129–138. <https://doi.org/10.1538/expanim.14-0059>
- Kumar V, Bhatt PC, Rahman M et al (2017a) Fabrication, optimization, and characterization of umbelliferone  $\beta$ -D-galactopyranoside-loaded PLGA nanoparticles in treatment of hepatocellular carcinoma: in vitro and in vivo studies. *Int J Nanomed* 12:6747–6758. <https://doi.org/10.2147/IJN.S136629>
- Kumar V, Bhatt PC, Rahman M et al (2017b) Umbelliferon- $\alpha$ -D-glucopyranosyl-(2 I  $\rightarrow$  1 II)- $\alpha$ -D-glucopyranoside ameliorates diethylnitrosamine induced precancerous lesion development in liver via regulation of inflammation, hyperproliferation and antioxidant at pre-clinical stage. *Biomed Pharmacother* 94:834–842. <https://doi.org/10.1016/j.biopha.2017.07.047>
- Lengauer T, Lemmen C, Rarey M, Zimmermann M (2004) Novel technologies for virtual screening. *Drug Discov Today* 9:27–34
- Nishida N, Yano H, Nishida T et al (2006) Angiogenesis in cancer. *Vasc Health Risk Manag* 2:213–219
- Ou-Yang S, Lu J, Kong X et al (2012) Computational drug discovery. *Acta Pharmacol Sin* 33:1131–1140. <https://doi.org/10.1038/aps.2012.109>
- Patel RM, Patel SK (2011) Cytotoxic activity of methanolic extract of *Artocarpus heterophyllus* against a549, hela and mcf-7 cell lines. *J Appl Pharm Sci* 1:167–171

- Pettersen EF, Goddard TD, Huang CC et al (2004) UCSF chimera—a visualization system for exploratory research and analysis. *J Comput Chem* 25:1605–1612. <https://doi.org/10.1002/jcc.20084>
- Prager GW, Poettler M (2011) Angiogenesis in cancer. *Hamostaseologie* 32:105–114. <https://doi.org/10.5482/ha-1163>
- Rollinger JM, Stuppner H, Langer T (2008) Virtual screening for the discovery of bioactive natural products. *Prog Drug Res* 65(211):213–249. [https://doi.org/10.1007/978-3-7643-8117-2\\_6](https://doi.org/10.1007/978-3-7643-8117-2_6)
- Siegel RL, Miller KD, Jemal A (2016) Cancer statistics. *CA Cancer J Clin* 66:7–30. <https://doi.org/10.3322/caac.21332>
- Singh D, Singh M, Yadav E et al (2018) RSC Advances knockdown oxidative stress and proinflammatory markers by *Madhuca longifolia* embedded silver nanoparticles. *RSC Adv* 8:6940–6953. <https://doi.org/10.1039/C7RA12775H>
- Srivastava JK, Pillai GG, Bhat HR et al (2017) Design and discovery of novel monastrol-1, 3, 5-triazines as potent anti-breast cancer agent via attenuating epidermal growth factor receptor tyrosine kinase. *Scientific Reports* 7:5851. <https://doi.org/10.1038/s41598-017-05934-5>
- Sys GML, Lapeire L, Stevens N et al (2013) The in ovo CAM-assay as a xenograft model for sarcoma. *J Vis Exp* 77:e50522. <https://doi.org/10.3791/50522>
- Tonini T, Rossi F, Claudio PP (2003) Molecular basis of angiogenesis and cancer. *Oncogene* 22:6549–6556. <https://doi.org/10.1038/sj.onc.1206816>
- Verma A, Bhatt PC, Kaithwas G et al (2016) Chemomodulatory effect *Melastoma Malabathricum* Linn against chemically induced renal carcinogenesis rats via attenuation of inflammation, oxidative stress, and early markers of tumor expansion. *Inflammopharmacology* 24:233–251. <https://doi.org/10.1007/s10787-016-0276-1>
- Verma A, Ahmed B, Anwar F et al (2017a) Novel glycoside from *Wedelia calendulacea* inhibits diethyl nitrosamine-induced renal cancer via downregulating the COX-2 and PEG<sub>2</sub> through nuclear factor- $\kappa$ B pathway. *Inflammopharmacology*. <https://doi.org/10.1007/s10787-017-0310-y>
- Verma A, Singh D, Anwar F et al (2017b) Triterpenoids principle of *Wedelia calendulacea* attenuated diethylnitrosamine-induced hepatocellular carcinoma via down-regulating oxidative stress, inflammation and pathology via NF- $\kappa$ B pathway. *Inflammopharmacology*. <https://doi.org/10.1007/s10787-017-0350-3>
- Wang MH, Kao MF, Jang LS (2011) Single HeLa and MCF-7 cell measurement using minimized impedance spectroscopy and microfluidic device. *Rev Sci Instrum* 82(6):064302. <https://doi.org/10.1063/1.3594550>
- Weis SM, Cheresh DA (2011) Tumor angiogenesis: molecular pathways and therapeutic targets. *Nat Med* 17:1359–1370. <https://doi.org/10.1038/nm.2537>
- World Health Organization (2012) WHO. World Health Statistics 2012, Geneva
- World Health Organization, Cancer Research UK (2014) World cancer factsheet. *World Heal Organ* 2012:4. <https://doi.org/10.1002/ijc.27711>
- Yang Y, Sun M, Wang L, Jiao B (2013) HIFs, angiogenesis, and cancer. *J Cell Biochem* 114:967–974. <https://doi.org/10.1002/jcb.24438>